

Article

Validation of Selected Optical Methods for Assessing Polyethylene (PE) Liners Used in High Pressure Vessels for Hydrogen Storage

Paweł Gašior^{1,*} , Karol Wachtarczyk¹ , Aleksander Błachut¹, Jerzy Kaleta¹, Neha Yadav², Marcin Ozga³ and Amelie Baron⁴

- ¹ Department of Mechanics, Materials and Biomedical Engineering, Wrocław University of Science and Technology, 50-370 Wrocław, Poland; karol.wachtarczyk@pwr.edu.pl (K.W.); aleksander.blachut@pwr.edu.pl (A.B.); jerzy.kaleta@pwr.edu.pl (J.K.)
- ² Department of Polymer Engineering, University of Leoben, 8700 Leoben, Austria; neha.yadav@unileoben.ac.at
- ³ Keyence International, 2800 Mechelen, Belgium; m.ozga@keyence.eu
- ⁴ RAIGI SA, 28310 Rouvray-Saint-Denis, France; baron.amelie@raigi.com
- * Correspondence: pawel.gasior@pwr.edu.pl; Tel.: +48-71-320-3919

Featured Application: The proposed assessing method can find an application for the non-destructive evaluation of PE liners at the beginning of the manufacturing chain of high-pressure composite vessels for hydrogen storage. It can be a low-cost method supporting visual inspection, which is presently the main tool used.



Citation: Gašior, P.; Wachtarczyk, K.; Błachut, A.; Kaleta, J.; Yadav, N.; Ozga, M.; Baron, A. Validation of Selected Optical Methods for Assessing Polyethylene (PE) Liners Used in High Pressure Vessels for Hydrogen Storage. *Appl. Sci.* **2021**, *11*, 5667. <https://doi.org/10.3390/app11125667>

Academic Editor:
Giuseppe Lacidogna

Received: 13 May 2021
Accepted: 15 June 2021
Published: 18 June 2021

Publisher's Note: MDPI stays neutral with regard to jurisdictional claims in published maps and institutional affiliations.

Abstract: A polyethylene (PE) liner is the basic element in high-pressure type 4 composite vessels designed for hydrogen or compressed natural gas (CNG) storage systems. Liner defects may result in the elimination of the whole vessel from use, which is very expensive, both at the manufacturing and exploitation stage. The goal is, therefore, the development of efficient non-destructive testing (NDT) methods to test a liner immediately after its manufacturing, before applying a composite reinforcement. It should be noted that the current regulations, codes and standards (RC&S) do not specify liner testing methods after manufacturing. It was considered especially important to find a way of locating and assessing the size of air bubbles and inclusions, and the field of deformations in liner walls. It was also expected that these methods would be easily applicable to mass-produced liners. The paper proposes the use of three optical methods, namely, visual inspection, digital image correlation (DIC), and optical fiber sensing based on Bragg gratings (FBG). Deformation measurements are validated with finite element analysis (FEA). The tested object was a prototype of a hydrogen liner for high-pressure storage (700 bar). The mentioned optical methods were used to identify defects and measure deformations.

Keywords: non-destructive evaluation; PE liner; high-pressure vessel; hydrogen storage; optical fiber sensors; digital image correlation



Copyright: © 2021 by the authors. Licensee MDPI, Basel, Switzerland. This article is an open access article distributed under the terms and conditions of the Creative Commons Attribution (CC BY) license (<https://creativecommons.org/licenses/by/4.0/>).

1. Introduction

1.1. Liner's Role in the Pressure Storage of Hydrogen

The acquisition of electric energy from fuel cells combined with hydrogen vessels is an alternative solution to the use of lithium-ion batteries and, simultaneously, one of the key stages in the technological development of energy supply for equipment, mobile devices, and stationary objects. Hydrogen, being an energy carrier used in the power supply to fuel cells, can be used in three states of matter: gas, liquid, or a chemically bonded phase in solids and liquids. Its storage form depends on the state of matter, the most frequently used solution being the storage of compressed gas.

In pressure storage systems (Figure 1), from 35 to 70 MPa, the most technologically advanced and safest solutions are applied, thus they have a well-deserved high reputation resulting from their use in transport, mainly over land and water, in stationary systems used for energy generation and hydrogen storage, including systems cooperating with renewable energy sources (RES). This is because high-pressure systems, and especially composite vessels, are highly efficient, i.e., the values of parameters describing the amount of stored hydrogen or energy in relation to the mass or volume of a storage system (expressed as system gravimetric capacity or system volumetric capacity, respectively). Moreover, despite the use of high working pressures, they are characterized by a high exploitation safety owing to the fact that they meet the strict requirements specified in binding regulations. In comparison with other hydrogen storage methods, e.g., various chemical absorption methods and liquid hydrogen at cryogenic temperatures, they are also competitively priced.

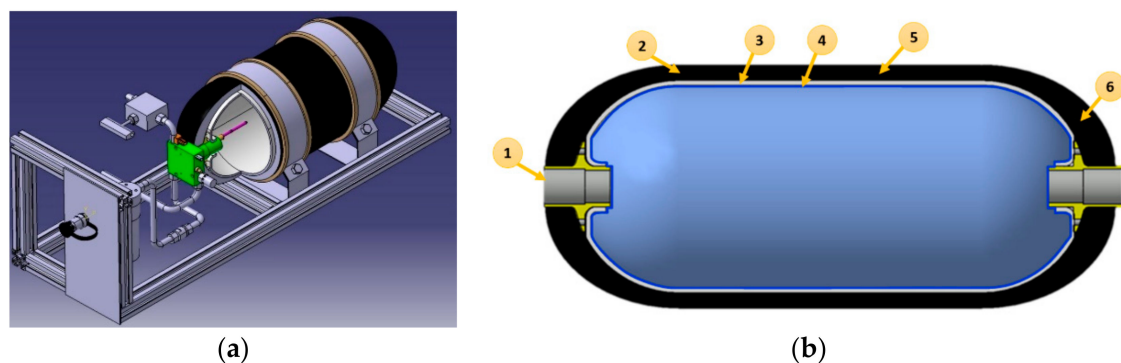


Figure 1. Scheme of a high-pressure hydrogen storage vessel. (a) A cross section and (b) a construction scheme: 1—inlet boss, 2—composite load carrying shell, 3—liner, 4—permeation reducing sol-gel coating, 5—cylindrical part, 6—dome with visible PE liner inside.

Composite vessels used for compressed gas storage are composed of two layers (Figure 1). The internal layer (the so-called liner) is responsible for gas accumulation and shaping the whole construction. It must form a barrier that is sufficiently strong to prevent gas particles from permeating outside the container. The liner can be made of metal (suitable steel type or aluminum alloys) or plastics (polymers). Currently, the latter solution tends to dominate. This results mainly from the following requirements, which modern liners must meet:

- The smallest possible mass of a hydrogen storage system, which can only be ensured by using completely composite containers (type 4) in which a liner is made of a polymer and a load-carrying shell is made of woven carbon fiber;
- The smallest hydrogen permeability, thanks to the use of high-density materials and additional sealing with, e.g., sol-gel type of materials [1];
- Ease of formation and geometry modification, due to the use of polymer technology solutions, which have been known for many years, such as rotomolding, blow molding, or extrusion;
- Low reactivity to hydrogen, i.e., small influence of stored gas on material properties (e.g., elimination of the hydrogen corrosion problem that occurs in the case of metal liners).

1.2. Liner in High Pressure Composite Vessel: Materials and Manufacturing Process

From the perspective of the exploitation of a type 4 high-pressure vessel, the most critical element is the liner. It is directly responsible for the accumulation of gaseous hydrogen; thus, its tightness is of paramount importance. In accordance with binding standards, hydrogen permeation through container walls is permitted as long as it does not exceed 6 Ncm^3 per hour of hydrogen, per liter of the internal volume of the container [2]

or is <46 mL/h/L water capacity of the storage system in the case of a container meeting type-approval requirements [3]. In addition to this, the current regulations, codes and standards (RC&S) specify that the materials used to make a container, including the liner, must exhibit so-called hydrogen compatibility pursuant to [4]. For more information on the influence of hydrogen on polymers, see the literature studies below.

Simultaneously, the liner performs the role of a core in the composite layer winding process, which determines the final strength of the construction. Most frequently, the liner has the shape of a cylinder with non-spherical geometry domes. The liner also contains metal bosses that allow fixing pressure valves and a connection between the container and the gas installation. A boss can also be used as a mounting grip (in the so-called neck mounting system). The liner can be made of metal (appropriate steel types or aluminum alloys). However, in the most technologically advanced containers, liners are only made of polymers (Figure 2). Then, the dominant materials used to make the liner are: high-density polyethylene (HDPE), polyamide (PA6) or, not so frequently, PET, polyoxymethylene (POM), and ethylene vinyl alcohol copolymer (EVOH) [5,6].



Figure 2. View of the exemplary HDPE liner for a hydrogen vessel, manufactured using rotomolding technology.

Despite the fact that the manufacturing cost of a liner, in comparison with that of the whole container, is relatively low and under series production conditions, it does not exceed 10% of the cost to make a high-quality liner; one needs an expensive machine park, as well as specialist knowledge on the materials and their processing technology.

Usually, a liner is produced by extrusion, rotomolding or blow molding, or some combination of these, through the use of the plastic jointing technique, i.e., bonding of extruded domes with an integrated boss with extruded tubes [7]. Metallic bosses can also be integrated within the domes by gluing them directly to the liner in a second step [8]. Below, short descriptions of two manufacturing methods are given.

One of the most commonly used technologies in liner production is rotomolding, in which a final product is formed in a mold by simultaneously rotating and raising the temperature to about 200 °C. First, metal bosses and polymer (e.g., HDPE, PA) in the form of a granulate are placed in a mold that is used to make the liners. During the process, the input material settles on the mold walls, which make the external geometry of the liner. The thickness of the liner walls is controlled by the amount of granulate put into the mold and the program controlling the machine motion. During the cooling stage, which lasts until ambient temperature is reached inside the mold, a massive pressure pushes the walls of the newly made liner against the mold walls, thus preventing collapse during a contraction. After the cooling process, the finished product is removed from the mold and requires only quality control and mechanical processing of the sealing surfaces near the boss. The fundamental advantages of rotomolding are the lack of connections and welds on the liner and no internal tensions in the construction, regulated wall thickness, and easy formation of additional elements (threaded elements, bosses, etc.). Rotomolding is also the most economical process in multi-series production and is completely automated.

Some manufacturers of containers prefer liners made using plastic jointing technology, which is thermal welding of a pipe forming the cylindrical part of a pressure vessel with ready domes. The most significant advantage of this method is the free choice of the final

size/internal volume of a pressure vessel, independent of the size of the mold (which is the case in rotomolding).

1.3. Polymer Liners—State-of-the-Art (SoA) in Manufacturing and Exploitation Related Issues

The literature devoted to polymer liners used for hydrogen storage in type 4 containers is extensive and encompasses a large number of issues. Below, mainly material and technology-related problems influencing liner stability and hydrogen permeability were selected and are indicated:

- Polymer aging and thermal degradation [5,9];
- Chemical structure, including molecular weight and molecular weight distribution of polymer chains [5,8–10];
- The degree of crystallinity of a polymer, which is affected by its cooling rate from the molten state [9–11];
- Processing techniques that can induce the orientation and extension of polymer chains affecting various properties) [5,9];
- The types and amounts of plasticizers, fillers, crosslinking agents, and other additives that are often incorporated to modify polymer properties [5,9–11];
- Influence of long-term high-pressure hydrogen exposure on the physical properties and mechanical performance of polymers [10,12,13];
- Hydrogen permeability of polymers as a result of diffusivity and solubility [5,8,14–17];
- Permeation rates, which are strongly dependent on the glass transition temperature [8, 10,11,16,18];
- Parameters responsible for the liner collapse in hyperbaric type 4 hydrogen storage vessels [14,19–22];
- Blistering resulting from hydrogen sorption and the subsequent decompression of a hydrogen container [8,9,11,14,22,23];
- Standardization of materials, container manufacturing, and testing technology, including liners [24];
- Limiting hydrogen permeability (e.g., by the use of barrier layers made using sol-gel technology, e.g., [1,25–27]), or the use of constructions limiting the amount of hydrogen accumulated between a liner and composite (reduction of the so-called air gaps, or also the use of ventilation structures inside composites to allow natural hydrogen escape);
- Liner resistance to high temperature, e.g., when a fire occurs near a high-pressure hydrogen storage container [28,29]. An additional goal is the so-called controlled defect, which allows for heat transfer through a composite shell and leads to liner melting [9,28]. Then hydrogen accumulated inside the container leaks through pores in the liner, which, in such a case, grow in size, but it combusts immediately on the container surface, thus ensuring safety.

2. Hydraulic Tests of Type 4 Containers, Motivation for Research and Goals

In the case of type 4 containers, the dominating failure mode is directly related to the liner. Despite its low price, if a liner is faulty, it eliminates a significantly more expensive product from use, i.e., the whole container. Some liner defects result from errors in the manufacturing technology, limitations related to the used material or design, and exploitation errors related to the whole container. On the other hand, a liner defect may contribute to the occurrence of phenomena, such as blistering, buckling, aging, or increased hydrogen permeability, later when in contact with hydrogen.

Every new type 4 container construction first undergoes hydraulic tests: static and fatigue tests. The cost of a necessary series of tests is high; however, it is known, from the many years of research by the authors of this paper, that in the hydraulic tests of a finished container, especially a new one, a negative test result is usually obtained due to a faulty liner.

Below are some selected examples of liner defects detected as a result of the authors' own research on type 4 hydrogen high-pressure containers. Defects were usually related to:

- Air bubbles and other inclusions in the liner material;
- Non-homogeneity of liner geometry and wall thickness;
- Residual stress in the polymer after the liner production process;
- Cracks in the liner material resulting from cyclic loads (Figure 3);
- Cracks in the liner material resulting from low temperatures, below $-40\text{ }^{\circ}\text{C}$ (Figure 4);
- Defects in the area of the liner/boss joint;
- Fatigue cracks in the area of a metal boss (Figure 5).

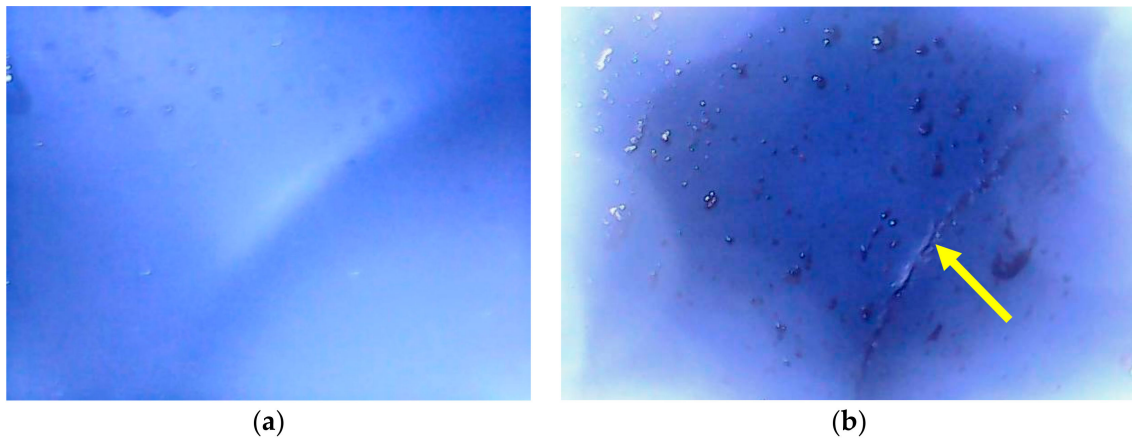


Figure 3. Endoscopy pictures of a defective liner. (a) The inlet dome area without visible cracks and (b) the outlet dome area with cracks around the boss–dome interface (marked by an arrow).

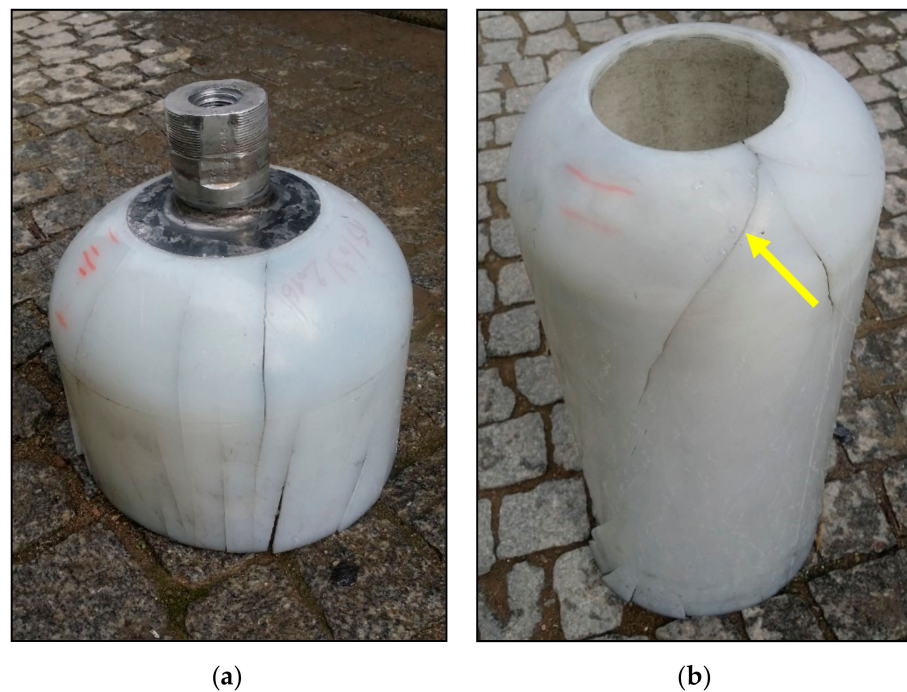


Figure 4. PE liner with major cracks extracted from a 700-bar hydrogen vessel after cyclic pressure test at low temperature. (a) Cut-off dome with the inlet boss and (b) the liner without the boss, which fell off due to the cracks at the liner material interface.



Figure 5. View of a damaged boss after fatigue testing. (a) Crack in the metallic boss and (b) crack in the inner side of the liner's dome.

In the case of liner defect, the composite comprising the load-bearing surface of a container usually remains intact; however, fatigue cracks occur in the liner, usually located near the dome or at the joint between the dome and the cylindrical part. There are also defects in the area of the connection between a boss and the liner material or, less frequently, boss defects resulting from fatigue cracks in the material.

At the development stage of new container construction, defects may be caused by both technological errors in the production of the liner itself or an incorrect design of the load-bearing overwrap. The non-uniform stress distribution in the composite layer of the construction may result in a local concentration of stress in the whole construction, which, in turn, can initiate cracks directly in the liner. In a previous study, unoptimized stress distribution in the geometry of a composite structure was observed and, as a consequence, the liner cracked during an ambient-temperature pressure cycle test in the 20–875-bar pressure range (Figure 6).

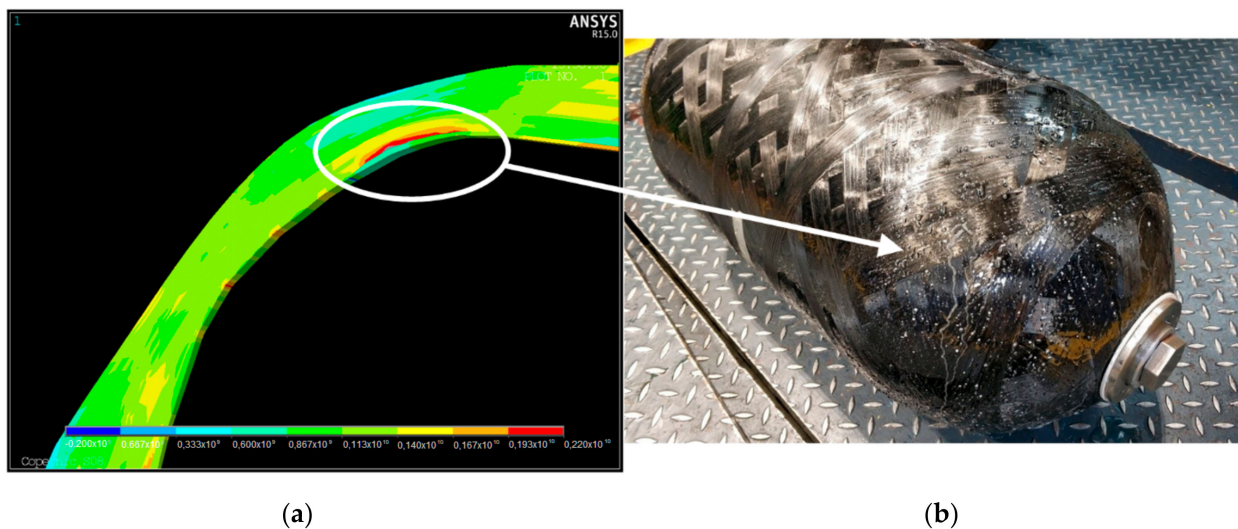


Figure 6. A 5-degree segment of the vessel model (ANSYS V15) presented normal stress (fiber orientation direction) in the composite material; (a) hotspot located in the dome area was the reason for liner damage and medium leakage [30]. (b) View of the leaking hydrogen vessel during the hydraulic test due to the cracks in the PE liner in the outlet dome area (water drops on the dome surface leaking through the pores in the composite shell).

Errors related to incorrect container design, both in the area of the boss or liner and a composite reinforcement, can be verified at the stage of introductory/qualification research (numerical and/or hydraulic tests of finished containers) and should not cause exploitation problems in certified containers. Approval for use in the case of containers means that they have successfully completed a whole cycle of tests at the type-approval stage; this is why, provided that the production procedures are repeatable, defects related to an incorrect construction design should not occur during normal exploitation. On the other hand, errors directly related to the liner production stage may not be detectable during type-approval and can occur later during day-to-day use of a container. At that time, however, the consequences of defects can be catastrophic.

To summarize, a properly manufactured liner is of key significance for the whole production process of a high-pressure composite container. Hence, if an efficient way of testing the liner itself were developed, i.e., testing it immediately after it was made and before applying a composite coating, the cost of negative consequences could be significantly reduced. It should be emphasized that current RC&S does not specify necessary liner tests that should be conducted after manufacturing. There are also no primary sources in this respect.

This is why there is a pressing necessity to develop non-destructive evaluation (NDE) methods for liners, to be applied immediately after the production process, to detect defects at an early stage (e.g., air bubbles and other inclusions, lack of homogeneity of liner geometry and wall thickness, residual stress in the polymer, cracks, and defects at the liner/boss joint).

With the above-mentioned in mind, it was assumed that the goal of this work would be to present the suitability of selected optical NDE methods for the assessment and analysis of liner operation, both at the product research and development stages (fiber Bragg gratings (FBG), digital image correlation (DIC)) and at the production stage (visual inspection).

3. Experimental Methods and Numerical Verification

The liner was investigated using two types of methods: visual defectoscopy and strain field analysis. Defectoscopy was performed by visual inspection, while the strain field analysis was done using two complementary methods—digital image correlation and fiber sensing based on Bragg gratings. Strain field measurements were further validated using the finite element method (FEM).

Visual inspection was used to verify its usefulness for liner evaluation after manufacturing. Liners produced by a rotomolding process can include air bubbles and inclusions in their structures, which can accelerate the degradation of a pressure vessel. Because of the semitransparency of HDPE, visual inspection was used to find those types of defects. On the other hand, translucent materials are more challenging for visual inspection than fully transparent ones.

The application of optical methods in the form of digital image correlation and optical fiber sensing based on FBG for high-pressure vessel monitoring has been widely described in numerous papers [31–36]. These methods can be used for performing full-field and local displacement/strain measurements, respectively. It has been proved that DIC can be effectively applied as a method for defect identification in a full field of view and that it can support an optimal localization of FBG sensors and their calibration. FBG sensors need to be integrated in the vessel structure to create an embedded structural health monitoring (SHM) system for composite high-pressure vessels. Within this paper, use of both of these methods was suggested to validate the behavior of the liner alone during pressure tests under laboratory conditions (R&D stage of the new product). The strain field measured with the complementary methods was validated using FEM. This way, manufacturing and design aspects were investigated.

3.1. Fiber Optical Sensors—Fiber Bragg Gratings

Fiber Bragg gratings are the most common optical fiber sensor used to measure strain and temperature changes. Thanks to their small size, they are common point-wise transducers that can also be easily integrated in a composite material (without any negative influence on its structure). The length of a single grating is in the range of 5–10 mm, and the external diameter is about 200–250 μm . Because of its excellent multiplexing capabilities, it is possible to combine many FBGs to form a network of sensors [31].

An FBG sensor has a specific structure formed in the core of an optical fiber, characterized by periodical changes in the refractive index value [37]. The measured value (deformation, temperature) is directly proportional to the displacement of the so-called Bragg wave (λ_B), which depends on a change in the grating period (Λ) resulting from the changes in fiber size (compressing, stretching) and thermal effects (thermal expansion of the material and the thermo-optic effect on the refractive index) [38].

3.2. Digital Image Correlation (DIC)

Digital image correlation is a well-established method for displacement, strains, and shape measurements [39]. Two-dimensional DIC (with one digital camera) and 3D DIC (with two or more digital cameras) are widely used and accepted in the field of experimental mechanics [40,41].

A straightforward measurement procedure requires acquiring a set of images of the object under investigation, which is subjected to any kind of load. One of the images is selected as the reference image (in most cases it is the image acquired before the load is applied) and the remaining images are subjected to correlation analysis. The reference image is divided into small sub-images or subsets. The subsets are subsequently matched against similar subsets in images acquired in different load states. Repeating the procedure for all subsets of the reference image yields displacement maps, which, in following steps, can be used for the calculation of strains. To allow the application of the DIC method, the object under investigation has to exhibit a random texture (speckle pattern) on its surface. In most cases, the speckle pattern is introduced on an object surface by spraying on paint [31].

3.3. Finite Element Method

The finite element method is the most commonly used technique to solve practical problems and mathematical models.

Clough [42] presented the idea of finite element analysis as a computational method used to find approximate results of boundary value problems in engineering. It shows when a component failure wears out or performs the way it was made to. It is used in the process of design and development to predetermine what will happen when a product is being used.

The idea of FEM was originally created by members of the structural dynamics unit at the Boeing Airplane Company. The main feature of the developed procedure is the evaluation of the stiffness properties of structural elements based on the assumed places of displacement interpolation functions [43].

In the FEM procedure, the three main steps are: (1) pre-processing—the creation of a finite element mesh. In the computational method, any type of material can be used with user-defined properties and boundary conditions. (2) Solution—the computational software used for the finite element analysis originates the matrix equations from the geometrical model and individually solves for the key measures. (3) Post-processing—an examination of the results of all primary quantities, such as displacement in a particular direction, which are obtained after the solution.

4. Experimental Tests of the Polymer Liner

The methods presented in the previous paragraph were used to test a commercial liner designed for high-pressure hydrogen storage vessels. It was made of high-density

polyethylene (HDPE) and manufactured using a rotomolding process (Figure 2). It had two steel inlet bosses, a total length of 80 cm, and a volume of 60 L. The cylindrical part was 55 cm long.

The liner was first inspected using a visual system. In the next step, FBG sensors were attached to the surface and a speckle pattern for DIC tests was sprayed onto the surface. The prepared liner was tested during the inflation process. This section describes the methods used in the liner testing in more detail.

4.1. Visual Inspection

The goal of the visual inspection was to find any defects caused by the manufacturing process (inclusions, air bubbles). Since HDPE is semi-transparent material, a method similar to candling was used to detect defects inside the material. To find defects, a setup made from a CMOS camera (CA-H500MX) with a CA-LHE16 lens and a ring-shaped multi-spectral light (CA-DRM20X) was used.

Recorded images were processed in such a way that defects on the images could be automatically detected. During image pre-processing, contrast correction, brightness, and shading were used. Later, for defect detection, automatic functions were used

4.2. FBG Sensors

FBG sensors, the “bare fiber” type with an Ormocer[®] coating, were used in this research. They are characterized by the lack of an additional buffer coating, which improves the transfer of loading between a monitored object and a transducer. The optical fiber sensors were integrated with the object using X60 glue, which is a two-component adhesive for strain gauges. Before attaching the sensors, the surface was de-greased, and, locally, the paint coating enabling the DIC measurements was also removed. The sensors were attached pointwise at the two ends of the Bragg grating. Thanks to this approach, the local inhomogeneity of deformation along the sensor axis was averaged along with the distance between the attachment points. An interrogator (SI405 HBM) was used to record the signals; it allows taking measurements at a 5-Hz frequency and 1-pm accuracy (corresponding to a 2- μe accuracy).

The whole liner was covered with 11 sensors in total. The placement of the sensors is shown in Figure 7. The description of the placement is provided in Table 1. Six sensors were placed on the cylindrical part of the liner (three in the circumferential direction and three in the longitudinal direction). Five sensors were placed on the dome (four concentric and one longitudinal).

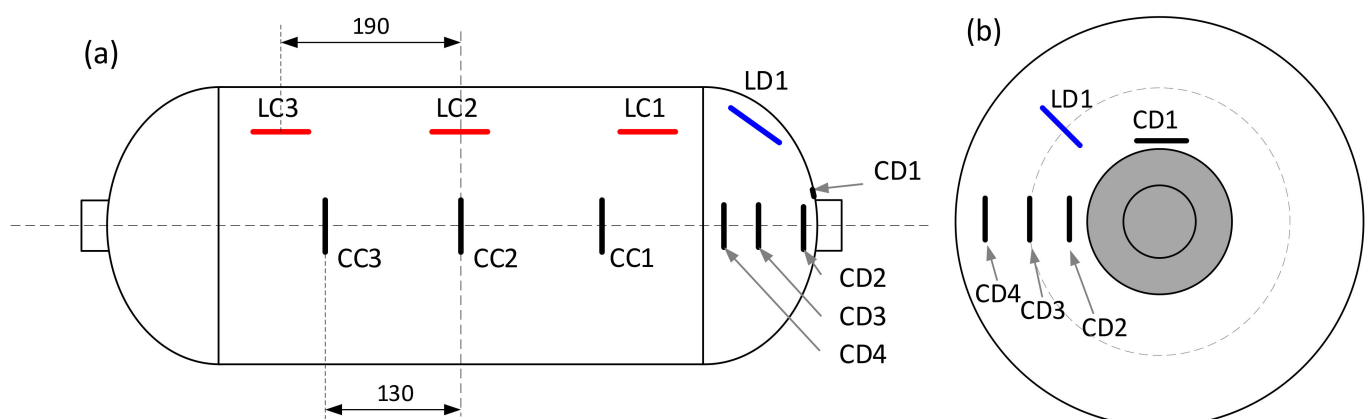


Figure 7. Placement of sensors on the liner. (a) Entire liner and (b) dome part. Colors are attributed to the different directions and locations of sensors: black—circumferential, red—longitudinal at the cylindrical part, blue—longitudinal at the dome.

Table 1. Description of the placement of optical strain sensors.

Direction	Location	Short Name	Description
Circumferential: C	Cylinder: C	CC1	Cylindrical part, circumferential, 130 mm from middle
		CC2	Cylindrical part, circumferential, central
		CC3	Cylindrical part, circumferential, symmetrical to CC1
Longitudinal: L	Cylinder: C	LD1	Dome, radial
		LC1	Cylindrical part, longitudinal, 190 mm from middle
		LC2	Cylindrical part, longitudinal, central
Circumferential: C	Dome: D	LC3	Cylindrical part, longitudinal, symmetrical to LC1
		CD1	Dome, 7 mm from boss, circumferential, placed next to gas bubbles
		CD2	Dome, 7 mm from boss, circumferential, placed in non-defected zone
		CD3	Dome, circumferential
		CD4	Dome, circumferential, close to the cylindrical part

4.3. DIC Method

As an additional measurement method, a 3D DIC system was used. The test setup is shown in Figure 8. The liner, after the placement of the sensors, was covered with a speckle pattern. The surface around the FBG sensors was cleaned so that the paint would not influence the sensor readouts. DIC system analysis was performed on a one-sided view of half the liner (one dome and 1/3 part of the cylindrical part, dashed line in Figure 8).

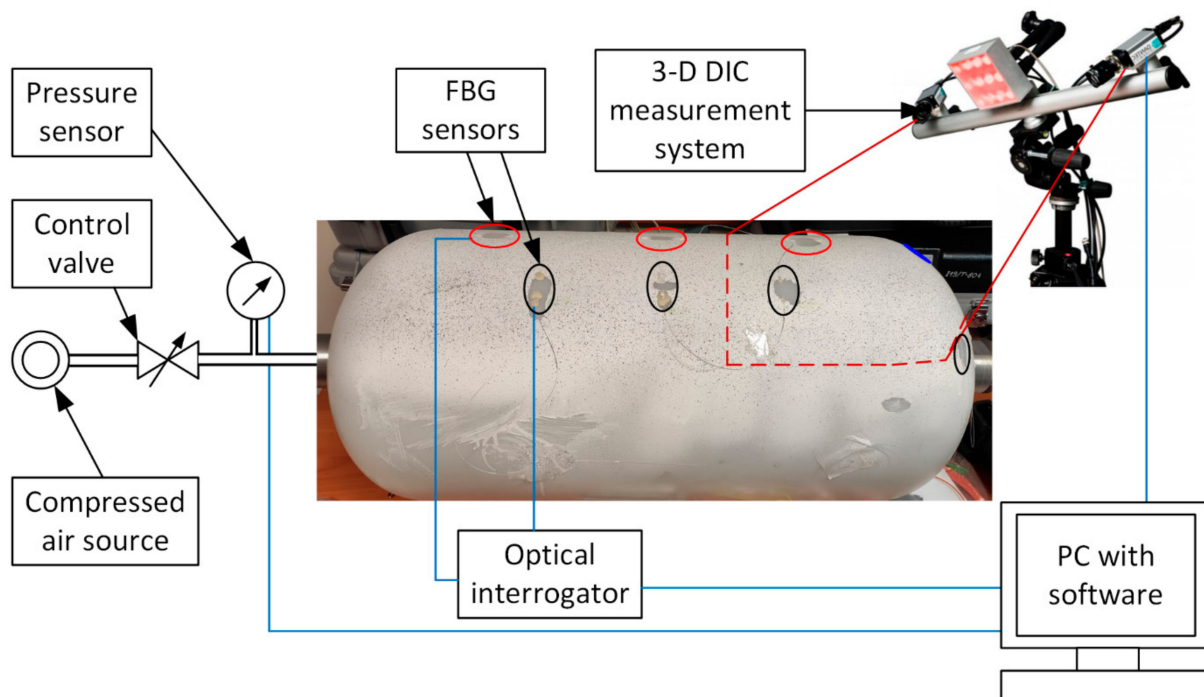


Figure 8. Experimental setup for liner testing using the DIC method and FBG sensors. Dashed line shows the part of the liner inspected using the DIC method.

The cameras for the DIC measurement system were mounted on a tripod, approximately 120 cm away from the vessel. The 3D DIC system was composed of two AVT Stingray 16Mpx cameras, equipped with lenses with a focal length of 50 mm and a PC using

Istra4D software. A typically obtained set of results from a single 3D DIC measurement was referenced to the Cartesian coordinate system and included the shape in the form of a cloud of points (x,y,z) , two components of in-plane displacements $(U(x,y), V(x,y))$, and an out-of-plane displacement map $(W(x,y))$.

The strain maps were calculated from the displacement maps in the 'xy' plane. Since the radii of curvature of a liner geometry were large and analysis was performed on a one-side view of the liner, it was assumed that ε_{xx} strain was strain along the circumferential direction, while ε_{yy} was in the longitudinal direction (along generation line). The validity of this approach was proven in [31].

To compare the results of the 3D DIC measurements and the FBG measurements, virtual extensometers were used. They were located in the displacement maps at the FBG locations. Their strain was calculated as the average strain between the sensor attachment points.

The experimental setup for the DIC test is presented in Figure 8. During the experiment, the liner was internally loaded with compressed air, with a pressure range from 0 to 1.3 bar. The pressure increase was controlled by a pressure gauge and a control valve.

4.4. FEA Model

The FEA model was prepared in the Abaqus/CAE environment and solved using the Abaqus 2020 static linear solver. The geometry was created based on the measured thickness of the test object and a 20-degree portion of the liner was modeled. High-density polyethylene and aluminum alloy were considered as linear elastic materials in the described analysis. The interface between the boss and the polymer was established using common nodes. C3D10 named elements were used in the model (ten-node quadratic tetrahedron). In the polymer material, dome area (close to the boss) defects were modeled as a discontinuity in the material, shown in Figure 9. The wall thickness along the generating line was measured post-mortem using a calliper. The liner was cut along the locations of the FBG sensors (first cut along LD1-LC-LC3 and the second along CC1-CC3).

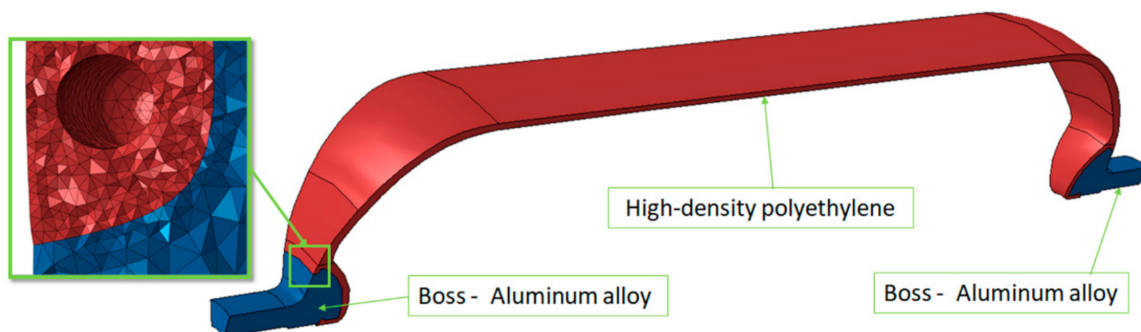


Figure 9. Liner model used in FEA with zoomed mesh around the porosity.

5. Results and Discussion

5.1. Visual Inspection

The detection of defects inside a structure requires lighting and image acquisition conditions that allow obtaining the highest possible contrast between the material and defects. In this case, the color and the type of lighting play the most significant roles. Inspection under various lighting conditions was possible thanks to a ring multi-spectrum light.

After determination of the best lighting conditions and the method for finding defects, the whole liner was inspected to find air bubbles, inclusions, and other defects.

In the cylindrical part and domes, a few individual and small (<1 mm) air bubbles were found. No agglomerations of air bubbles were observed. In close proximity to the boss, there were numerous air bubble chains with diameters of about 2 mm. The defect is shown in Figure 10. For automating the process of detecting production defects, the automatic detection methods available in Keyence CV-X Machine Vision System were used.

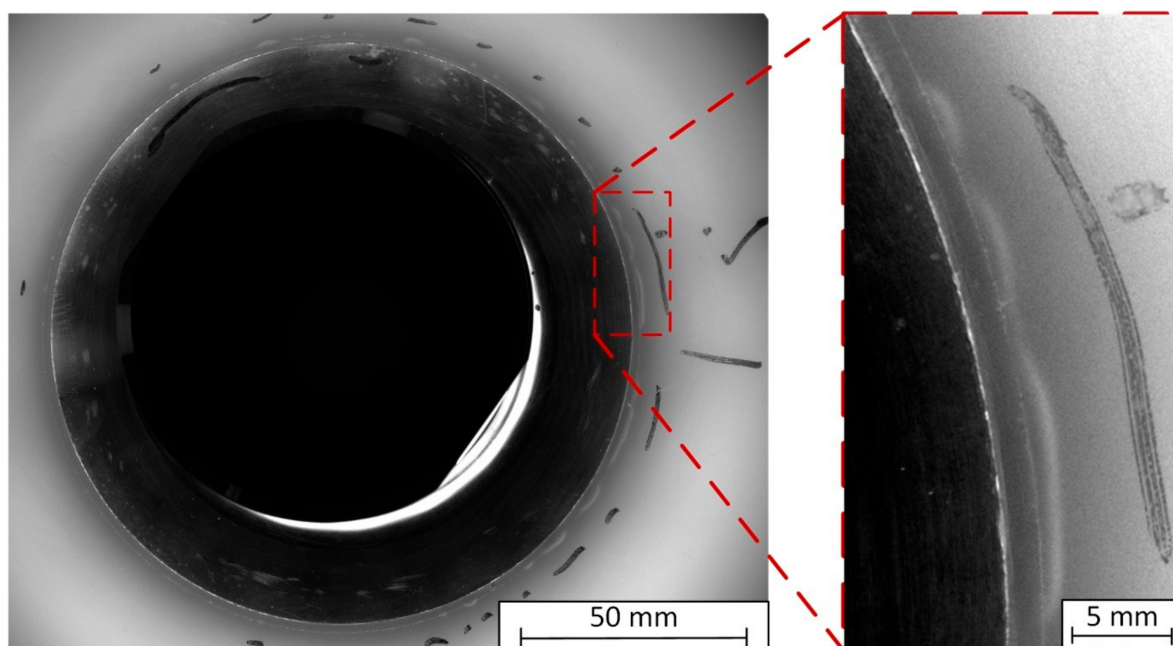


Figure 10. View of a liner's inlet with air chain located near the boss.

Experience related to pressure container tests suggests that this defect may lead to container faults during cyclic hydraulic loading (fatigue defects, leaks near the boss/HDPE interface) or to hydrogen accumulation during exploitation of a container. To investigate the influence of this defect on the strain field around the boss, FBG sensors were attached close to the boss (one near the defect and one near a non-defective area) and FEA analysis of this point was performed.

5.2. Deformation Measurement of the Liner

Investigation of the liner deformation field was conducted under internal loading conditions in a pressure range from 0 to 1.3 bar. Compressed air was used as a medium. The pressure rate was controlled by hand with a valve. After reaching maximum pressure, the air was gradually released.

Liner deformation was recorded using fiber Bragg gratings and a 3D DIC system. FBG provided data about point-wise deformations, while DIC was used for strain field measurements. FBGs were used for measurements during the entire test and DIC data were collected during the increasing of the internal pressure up to 1 bar. FEA validation was also performed for this pressure level.

5.2.1. Strain Measurements Using FBG Sensors

The measurement data obtained using FBG sensors were recorded while pumping in and releasing air from the liner. The locations of the sensors on the surface of the liner are described in Table 1 and presented in Figure 7. The results were recorded using 11 sensors. The results of deformation measurements during the tests are presented in Figure 11.

In Figure 11a there is visible slow loading of the liner with pressured air, which ended after 220 s. After this, air was slowly released until 440 s of experiment time. A non-constant pressure rate was caused by manual control of the inlet valve.

After the air was released, in Figure 11a, one can observe the occurrence of a delay in the liner's return to its initial deformation state. This means that the value of its internal pressure regained the value of the atmospheric pressure, despite the fact that the non-zero deformations of the material were still visible. The effect could be observed for as long as two minutes after releasing the air. Figure 11b (strain–pressure plot) shows mechanical hysteresis, which is typical for a visco-elastic material, such as HDPE.

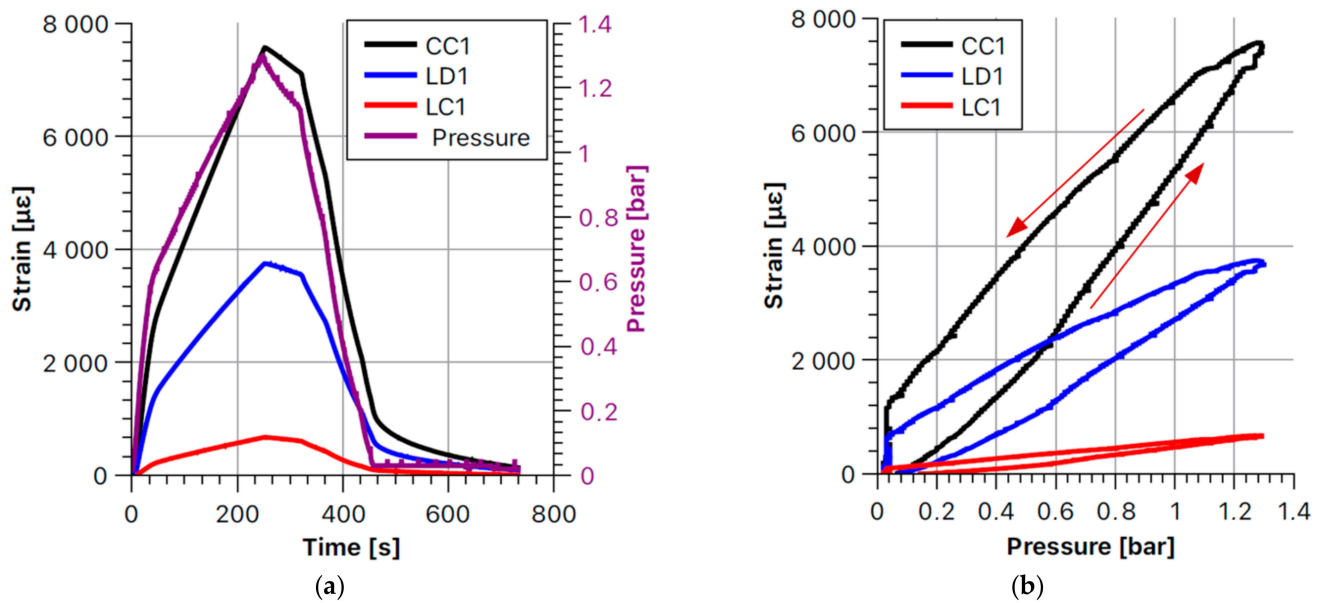


Figure 11. Deformation registered with selected FBG sensors. (a) Over time and (b) over pressure. Arrows show the direction of pressure increasing/decreasing.

To present the point-wise deformation state of the liner, deformation values registered by each sensor at 1 bar pressure are shown in Table 2.

Table 2. Strain registered by FBG sensors for 1-bar internal pressure.

Location/Sensor Number	1	2	3	4
CC	5460 μϵ	5530 μϵ	7080 μϵ	-
LC	480 μϵ	250 μϵ	740 μϵ	-
CD	300 μϵ	270 μϵ	470 μϵ	−20 μϵ
LD	2770 μϵ	-	-	-

In the case of sensors located on the cylindrical part of the liner, sensors CC1 and CC3, which were placed symmetrically to CC2, showed a 25% difference in circumferential strain. Because of the geometry, their values should be the same, but the most likely difference was caused by variations in the thickness of the walls. This hypothesis was validated using FEA based on post-mortem measurement of the wall thickness. A similar trend was visible for sensors placed in the longitudinal direction (LC1 and LC3). One side of the liner was deformed 50% more in the longitudinal direction. The highest deformation in the longitudinal direction was shown for sensor LD1, which was placed on the dome.

Sensors on the dome—CD1 and CD2—were in the same position relative to the boss, but sensor CD1 was located very close to the defect (air bubble chain). It was observed that the deformations near the defect were 10% larger than in the case without any defect.

Sensor CD4 was placed circumferentially on the dome and showed compression on the point on the dome. Further analyses in this paper show that this compression was caused by the liner's geometry.

5.2.2. Strain Field Distribution by DIC

The measurements taken using the DIC method were conducted in parallel to the measurements with FBG sensors while pumping air into the liner. The deformation field analyzed using the 3D-DIC system included a fragment of the dome and a fragment of the cylindrical part. The recorded deformation fields, ε_{xx} and ε_{yy} , at 1.0 bar are presented in

Figure 12. Along with the strain field obtained from the DIC method, the results from FEM are shown.

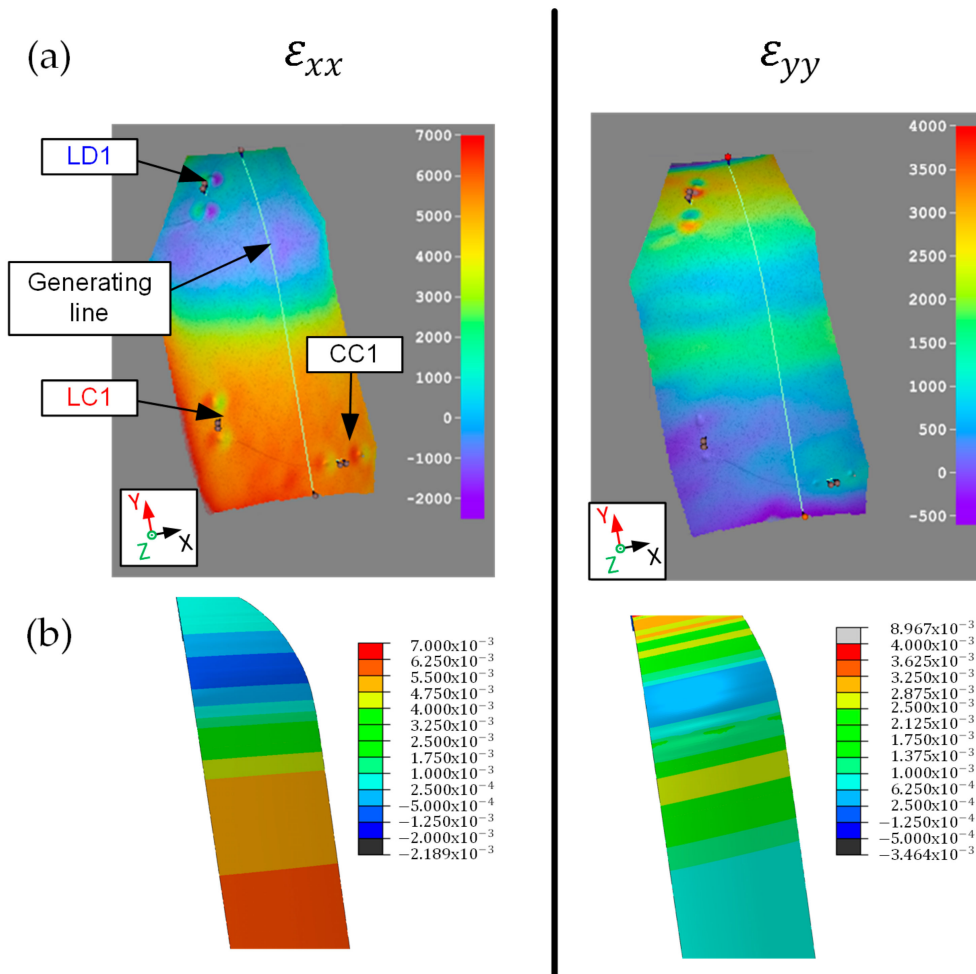


Figure 12. Deformation field in the circumferential and longitudinal direction at 1-bar pressure; (a) results of DIC tests and (b) FEM calculation.

Strain in the circumferential direction, ϵ_{xx} . (Figure 12a), had the highest value of around 7000 $\mu\epsilon$ on the cylinder part, closest to the middle of the liner (the bottom part of the presented photos). The circumferential strain of a dome was significantly smaller (<1000 $\mu\epsilon$). Measurement shown area with negative circumferential strain in the dome area (amplitude up to 100 $\mu\epsilon$). Strain in longitudinal direction ϵ_{yy} (Figure 12b) had maximum values on the dome (about 3500 $\mu\epsilon$).

In Figure 12, three FBG sensors are visible, which allows validating both methods. Results of FEM (bottom of Figure 12) are in accordance with the DIC results for both ϵ_{xx} and ϵ_{yy} directions.

The observation of compression in the circumferential direction was confirmed using FEA. Deformation of the liner from DIC and FEA along the generating line (marked in Figure 12) is shown in Figure 13.

Figure 13 shows good correlation between results from DIC and FEM for both ϵ_{xx} ϵ_{yy} and direction. Compression in circumferential direction was visible for both methods. The area of this behavior is present on the dome, close to the cylinder. Displacement around this area has almost two times lower deformation as the maximum deformation of cylinder and boss. It means that this behavior can be interpreted as the presence of the liner's collapse, which can potentially be a weak spot during vessel operation.

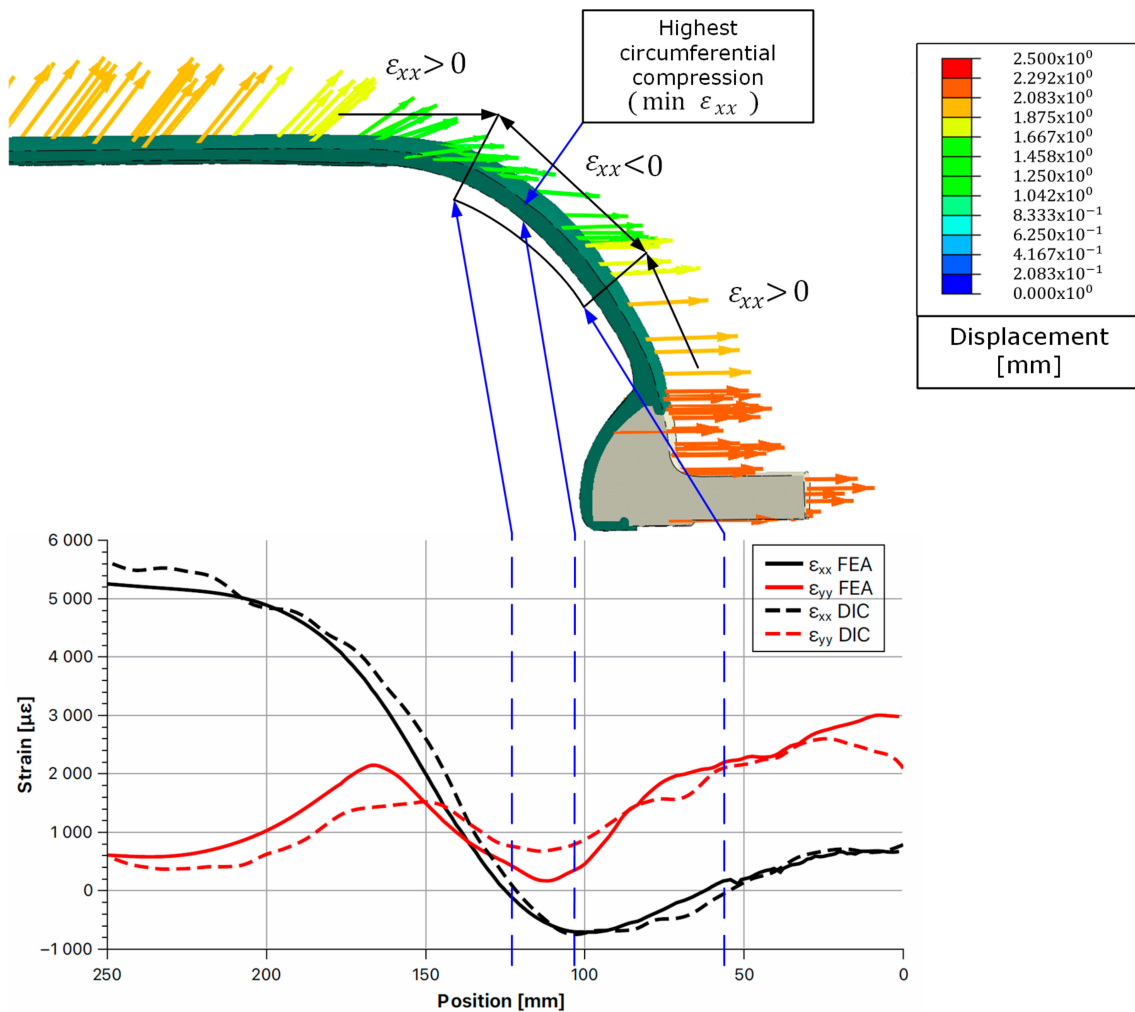


Figure 13. Strain in circumferential (ϵ_{xx}) and longitudinal (ϵ_{yy}) directions along the generating line using the DIC and FEM methods. Location of negative ϵ_{xx} area marked with arrows. Displacement of the liner shows collapse around this location.

It is worth noticing the visible non-homogeneity of the strain field. Some regions, even on the same cross-section, show non-uniform strain, which is attributed to thickness variations. Sensors attached to the surface of a liner could be placed in the areas where local strain non-homogeneity occurred. As a consequence, average strain measured by a sensor could be different in some local spots. This can be an explanation for the differences in the measurement results in Table 2.

5.2.3. FEA Strain Analysis

In addition to the dataset of strain on the dome part of the liner, strain along the cylindrical part of the liner and its fluctuations caused by thickness variations were investigated. After the testing, the liner was cut along the generating-line and the thickness of walls was measured 5 times every 20 mm with a calliper. The measured thickness of walls fluctuated from 4.50 mm to 6.03 mm. The closer to the dome the measurement was taken, the greater the thickness was; however, there was a measurable, average difference in the thickness on one half of the liner. The side of the CC1 and LC1 sensor had an average thickness of 0.2 mm higher than the thickness of side with the CC3 and LC3 sensors. The measured thicknesses of the liner's walls in the locations of sensors were as follows:

- Circumferential direction: CC1—5.02 mm, CC2—4.87 mm, CC3—4.68 mm,
- Longitudinal direction: LC1—5.08 mm, LC2—4.86 mm, LC3—4.82 mm.

In Figure 14, strain along the cylinder part of the liner with FBG sensor location indications (ϵ_{xx} and ϵ_{yy}) and strain along the generating line of the cylinder, along with marked locations of sensors, are shown. Results of FBG strain measurements were combined with data from FEM and are given in Table 3. The strain in the location of the FBG sensors was comparable with the results of the FEA based on real thickness measurements of the cylinder. This means that differences of strain are explainable by wall thickness variation, and thus by the manufacturing method.

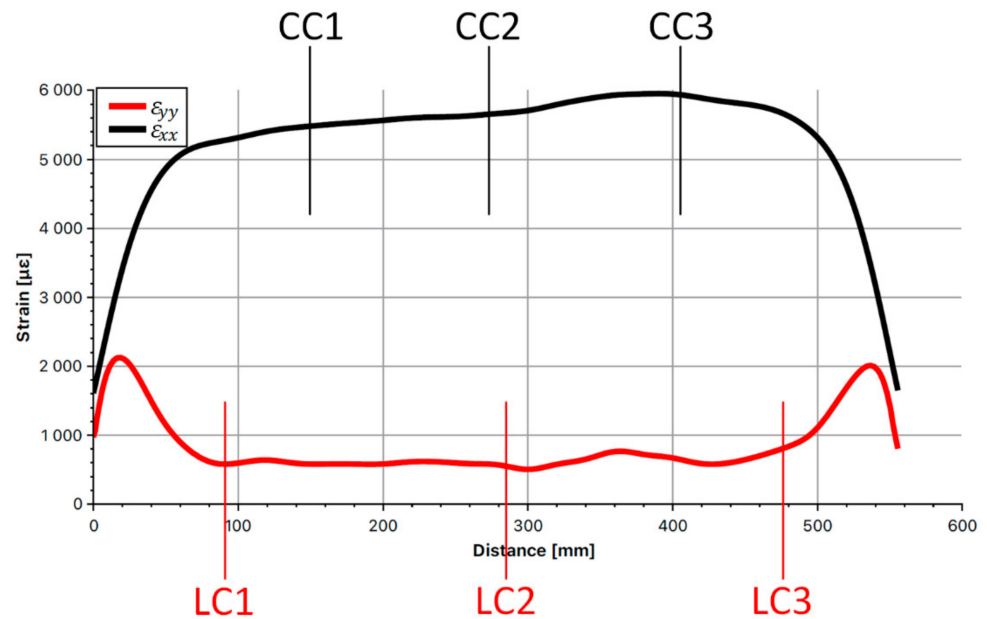


Figure 14. Strain along the cylinder part of the liner with FBG sensor location indication.

Table 3. Strain measured with FBG sensors compared with FEM results.

Sensor	FBG [$\mu\epsilon$]	FEM [$\mu\epsilon$]
CC1	5370	5400
CC2	5450	5600
CC3	6900	6000
LC1	480	580
LC2	240	500
LC3	730	790
CD1 (bubble)	300	351
CD2 (no bubble)	270	232

Authors investigated the influence of defects on the strain field in the area close to the dome: numerical simulation and point-wise strain measurements were used. Bragg sensors were glued about 7 mm from the liner's edge, the distance between the glue points was about 20 mm. The same area was analyzed by FEM using a tetrahedral mesh. Figure 15 shows the circumferential strain and the location of the strain sensor. The strain obtained from the numerical method was calculated based on the node displacement, of which locations correspond to the glue point and were compared with the strain measured by FBG (in Table 3). Figure 15a shows the circumferential strain for the dome without any defects; Figure 15b shows the circumferential strain for the dome with the defects modeled as an elliptical void. The location of the defect is shown in the wireframe model in Figure 15b,c.

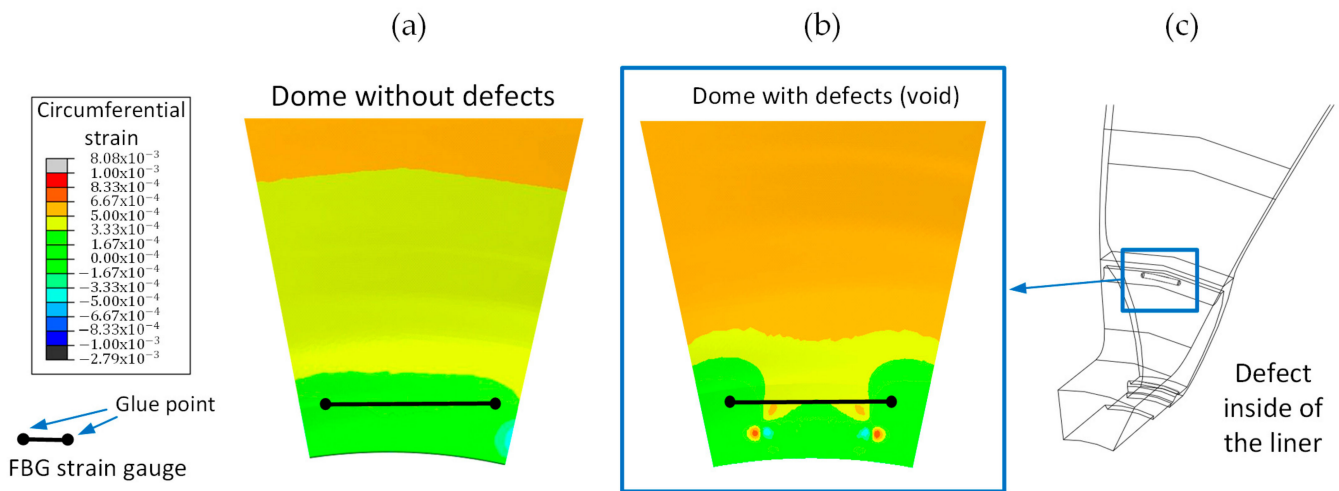


Figure 15. Strain field variations caused by the air-bubble chain located close to the boss: circumferential strain field distribution in the dome region model without defects (a) and with an internal defect in the form of the elliptical void (b), and location and geometry of the defect (c).

5.2.4. FBG, DIC, and FEA Result Comparisons

The results of DIC were compared with the values of deformation recorded using Bragg gratings. To achieve this goal, virtual extensometers of which the locations and directions were the same as the physical locations of the FBG sensors were used. Calculated strain from FEM was used for validation.

Due to the limitations of the DIC method, the results were compared for only three sensors. One of them was placed on the dome in the longitudinal direction (LD1) and two located on the cylindrical part (CC1—circumferential and LC1—longitudinal). The sensor’s location is marked in Figure 12.

A comparison of the results of the deformation measurements recorded using all methods is presented in Figure 16. Correlation is visible regardless of the direction of the measurement. The biggest relative error is visible for the longitudinal direction on the cylindrical part of the liner (LC1). For the circumferential direction of the cylinder part (CC1), the maximum relative error does not exceed 5%.

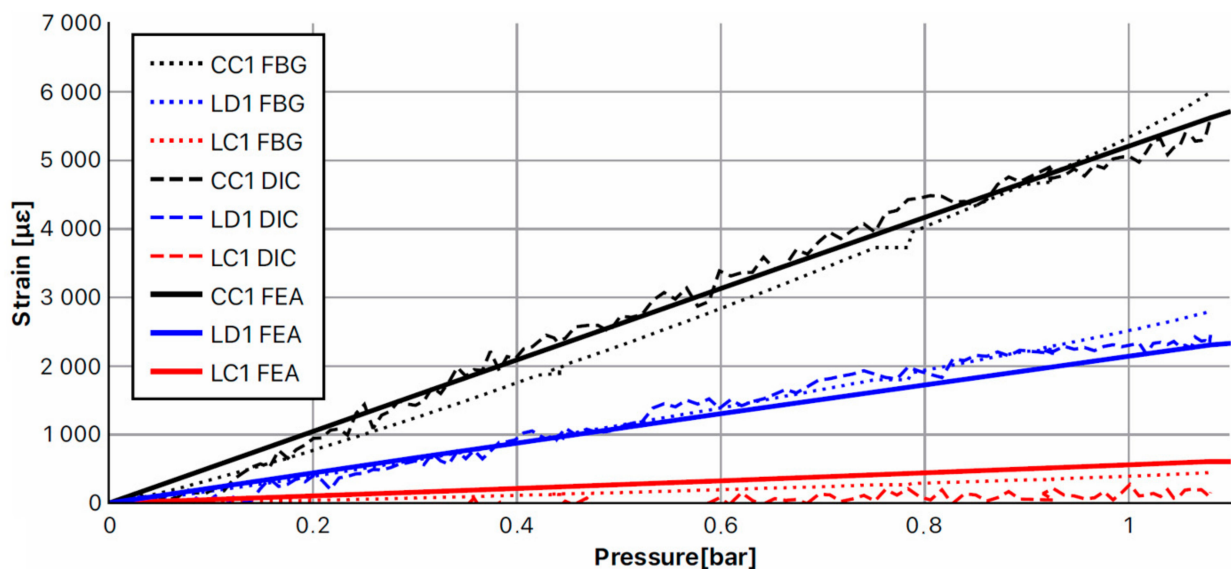


Figure 16. Chart presenting deformations recorded using FBG sensors, DIC method, and FEA model.

6. Summary

1. A correctly manufactured liner is of key importance in the whole process of the production and exploitation of a high-pressure type 4 composite vessel used for hydrogen storage. Although the manufacturing cost of a liner is relatively low in comparison to the whole vessel, any liner defects may lead to the elimination of a significantly more expensive vessel at its manufacturing or exploitation stage. Thus, it seems justified to develop an efficient method of testing the liner, i.e., right after its production, even before applying a composite coat. It should be noted that the current regulations, codes and standards (RC&S) do not specify liner testing methods after its manufacturing. There are also no primary sources in this respect.
2. The paper presents non-destructive evaluation (NDE) methods for liners to be applied immediately after the production process to detect defects at an early stage (e.g., air bubbles and other inclusions, lack of homogeneity of liner geometry and wall thickness, cracks and defects at the liner/boss joint). At the same time, the methods to be applied during the R&D stage in the form of digital image correlation (DIC), optical fiber sensing based on Bragg gratings (FBG), and visual inspection, were shown.
3. Visual inspection allows to detect defects occurring on both the domes and the cylindrical part of the liner. It enabled the observation of, e.g., air bubbles and inclusions in the liner walls. Moreover, this method can be completely automated for the qualitative assessment of liners at the manufacturing stage (detecting and locating air bubbles and other inclusions), thus allowing to test each object, even when mass-produced.
4. The DIC method and the usage of FBG sensors allow to determine circumferential and longitudinal deformations with high accuracy and are dedicated especially for prototype liners and R&D.
5. The strain field obtained with FBG sensors and the DIC method was confirmed with finite element analysis of the model. The liner's geometry was reconstructed with the measurements of the wall thickness. Correlation of measurement with all methods and confirmation by FEM means that the DIC method can be used for wall thickness perturbation and detection of non-homogenous strain fields (e.g., compression in the circumferential direction on a dome), which is caused by the design of a liner.

Author Contributions: Conceptualization, P.G. and J.K.; methodology, P.G.; software, K.W.; validation, A.B. (Aleksander Błachut) and K.W.; investigation, P.G., K.W., A.B. (Aleksander Błachut), N.Y. and M.O.; resources, A.B. (Amelie Baron); data curation, K.W.; writing—original draft preparation, J.K., P.G., K.W. and A.B. (Aleksander Błachut); writing—review and editing,—J.K., P.G., K.W. and A.B. (Aleksander Błachut); visualization, A.B. (Aleksander Błachut), K.W.; supervision, J.K.; funding acquisition, P.G. and J.K. All authors have read and agreed to the published version of the manuscript.

Funding: This research was co-financed by the Polish National Agency for Academic Exchange (PPN/BIL/2018/1/00058), and the statutory funds of the Wrocław University of Science and Technology.

Institutional Review Board Statement: Not applicable.

Informed Consent Statement: Not applicable.

Data Availability Statement: Data available on request due to restrictions eg privacy or ethical.

Acknowledgments: The calculations were made on computers Wrocław Center for Networking and Supercomputing (<http://www.wcss.pl>, accessed on 14 June 2021), Calculation Grant No. 419.

Conflicts of Interest: The authors declare no conflict of interest.

References

1. Szczurek, A.; Babiarczuk, B.; Kubacki, J.; Papin, P.; Renault, P.; Żak, A.; Kaleta, J.; Krzak, J. Sol-gel multilayered coatings for reduction of H₂ permeation. *Appl. Surf. Sci.* **2019**, *497*. [[CrossRef](#)]
2. Commission Regulation (EU) No 406/2010 of 26 April 2010 implementing Regulation (EC) No 79/2009 of the European Parliament and of the Council on Type-Approval of Hydrogen-Powered Motor Vehicles; Official Journal of the European Union: Brussels, Belgium, 2010.

3. Regulation No 134 of the Economic Commission for Europe of the United Nations (UN/ECE)—Uniform Provisions Concerning the Approval of Motor Vehicles and Their Components with Regard to the Safety-Related Performance of Hydrogen-Fuelled Vehicles (HFCV); Official Journal of the European Union: Brussels, Belgium, 2019.
4. *Transportable Gas Cylinders—Compatibility of Cylinder and Valve Materials with Gas Contents*; International Organization for Standardization: Geneva, Switzerland, 2017.
5. Barth, R.R.; Simmons, K.L.; San Marchi, C.W. *Polymers for Hydrogen Infrastructure and Vehicle Fuel Systems: Applications, Properties, and Gap Analysis*; Sandia National Laboratories: Albuquerque, NM, USA, 2013. [CrossRef]
6. Bigelow, E.; Lewis, M. *Conformable Hydrogen Storage Pressure Vessel*; Center for Transportation and the Environment: Atlanta, GA, USA, 2018. [CrossRef]
7. Anovitz, L.; Smith, B. *Lifecycle Verification of Tank Liner Polymers*; Oak Ridge National Lab. (ORNL): Oak Ridge, TN, USA, 2014. [CrossRef]
8. Barthelemy, H.; Weber, M.; Barbier, F. Hydrogen storage: Recent improvements and industrial perspectives. *Int. J. Hydrogen Energy* **2017**, *42*, 7254–7262. [CrossRef]
9. Azkarate, I.; Barthelemy, H.; Hooker, P.; Jordan, T.; Keller, J.; Markert, F.; Steen, M.; Tchouvelev, A. *Research Priorities Workshop on Hydrogen Safety*; Publications Office of the European Union: Luxembourg, 2018; ISBN 978-92-79-80975-0.
10. Menon, N.C.; Kruiuzenga, A.M.; San Marchi, C.W.; Campbell, J.; Nissen, A.; Mills, B.E. *Polymer Behaviour in High Pressure Hydrogen Helium and Argon Environments as Applicable to the Hydrogen Infrastructure*; Sandia National Laboratories: Albuquerque, NM, USA, 2017. Available online: <https://www.osti.gov/servlets/purl/1464594> (accessed on 14 June 2021).
11. Kane, M. *Permeability, Solubility, and Interaction of Hydrogen in Polymers—An Assessment of Materials for Hydrogen Transport*; Savannah River Site (SRS): Aiken, SC, USA, 2008.
12. Menon, N.C.; Kruiuzenga, A.M.; Alvine, K.J.; San Marchi, C.; Nissen, A.; Brooks, K. Behaviour of Polymers in High Pressure Environments as Applicable to the Hydrogen Infrastructure. In Proceedings of the ASME 2016 Pressure Vessels and Piping Conference, Vancouver, BC, Canada, 17–21 July 2016.
13. Menon, N.C.; Nissen, A.; Benton, J.T.; Campbell, J.; Mills, B.E. *Compatibility of Polymeric Materials in Hydrogen Service*; Sandia National Lab. (SNL-NM): Albuquerque, NM, USA, 2018.
14. Yersak, T.A.; Baker, D.R.; Yanagisawa, Y.; Slavik, S.; Immel, R.; Mack-Gardner, A.; Herrmann, M.; Cai, M. Predictive model for depressurization-induced blistering of type IV tank liners for hydrogen storage. *Int. J. Hydrogen Energy* **2017**, *42*, 28910–28917. [CrossRef]
15. Sperling, L.H. *Introduction to Physical Polymer Science*; John Wiley & Sons, Inc.: Hoboken, NJ, USA, 2005; ISBN 9780471757122.
16. Klopffer, M.H.; Flaconneche, B.; Odru, P. Transport properties of gas mixtures through polyethylene. *Plast. Rubber Compos.* **2007**, *36*, 184–189. [CrossRef]
17. Perreux, D.; Chapelle, D.; Nardin, P.; Thiébaud, F. Hydrogen Permeation Characteristics of PET Liners Used for Type IV High Pressure Hydrogen Tanks. *Mach. Dyn. Res.* **2013**, *37*, 85–97.
18. Brandrup, J.; Immergut, E.H.; Grulke, E.A.; Abe, A.; Bloch, D.R. (Eds.) *Polymer Handbook*, 4th ed.; John Wiley & Sons: New York, NY, USA, 1999; ISBN 978-0-471-16628-3.
19. Pepin, J.; Lainé, E.; Grandidier, J.C.; Castagnet, S.; Blanc-vannet, P.; Papin, P.; Weber, M. Determination of key parameters responsible for polymeric liner collapse in hyperbaric type IV hydrogen storage vessels. *Int. J. Hydrogen Energy* **2018**, *43*, 16386–16399. [CrossRef]
20. Pépin, J.; Lainé, E.; Grandidier, J.C.; Benoit, G.; Mellier, D.; Weber, M.; Langlois, C. Replication of liner collapse phenomenon observed in hyperbaric type IV hydrogen storage vessel by explosive decompression experiments. *Int. J. Hydrogen Energy* **2018**, *43*, 4671–4680. [CrossRef]
21. Blanc-Vannet, P.; Papin, P.; Weber, M.; Renault, P.; Pepin, J.; Lainé, E.; Tantchou, G.; Castagnet, S.; Grandidier, J.C. Sample scale testing method to prevent collapse of plastic liners in composite pressure vessels. *Int. J. Hydrogen Energy* **2019**, *4*, 8682–8691. [CrossRef]
22. Zhang, M.; Lv, H.; Kang, H.; Zhou, W.; Zhang, C. A literature review of failure prediction and analysis methods for composite high-pressure hydrogen storage tanks. *Int. J. Hydrogen Energy* **2019**, *44*, 25777–25799. [CrossRef]
23. Moradi, R.; Groth, K.M. Hydrogen storage and delivery: Review of the state-of-the-art technologies and risk and reliability analysis. *Int. J. Hydrogen Energy* **2019**, *44*, 12254–12269. [CrossRef]
24. Wang, D.; Liao, B.; Huang, G.; Hua, Z.; Gu, C.; Xu, P. Development of regulations, codes and standards on composite tanks for on-board gaseous hydrogen storage. *Int. J. Hydrogen Energy* **2019**, *44*, 22643–22653. [CrossRef]
25. Voloshchuk, I.; Zakroczymski, T. Hydrogen entry and absorption in ZrO₂ coated iron studied by electrochemical permeation and desorption techniques. *Int. J. Hydrogen Energy* **2012**, *37*, 1826–1835. [CrossRef]
26. Fukui, Y.; Katayama, T.; Mizuno, M. Hydrogen Tank Liner Material and Hydrogen Tank Liner. U.S. Patent 20090203845A1, 13 August 2009.
27. Andernach, R.; Lindner, T. Method to Improve the Barrier Properties of Composite Gas Cylinders and High Pressure Gas Cylinder Having Enhanced Barrier Properties. U.S. Patent 20130313266, 28 November 2013.
28. Halm, D.; Fouillen, F.; Lainé, E.; Gueguen, M.; Bertheau, D.; van Eekelen, T. Composite pressure vessels for hydrogen storage in fire conditions: Fire tests and burst simulation. *Int. J. Hydrogen Energy* **2017**, *42*, 20056–20070. [CrossRef]

29. Dadashzadeh, M.; Kashkarov, S.; Makarov, D.; Molkov, V. Risk assessment methodology for onboard hydrogen storage. *Int. J. Hydrogen Energy* **2018**. [[CrossRef](#)]
30. Nouven, G. Optimized designs of CPV's. In Proceedings of the Pressurized Hydrogen Storage and Equipment (PHASE 2016), Leuven, Belgium, 24–25 May 2016.
31. Gaşior, P.; Malesa, M.; Kaleta, J.; Kujawińska, M.; Malowany, K.; Rybczyński, R. Application of complementary optical methods for strain investigation in composite high pressure vessel. *Compos. Struct.* **2018**. [[CrossRef](#)]
32. Gasior, P.; Rybczynski, R.; Kaleta, J.; Villalonga, S.; Nony, F.; Magnier, C. High pressure composite vessel with integrated optical fiber sensors. Monitoring of manufacturing process and operation. *Am. Soc. Mech. Eng. Press. Vessel. Pip. Div. PVP* **2018**, *5*. [[CrossRef](#)]
33. Saeter, E.; Lasn, K.; Nony, F.; Echtermeyer, A.T. Embedded optical fibres for monitoring pressurization and impact of filament wound cylinders. *Compos. Struct.* **2019**, *210*, 608–617. [[CrossRef](#)]
34. Foedinger, R.C.; Rea, D.L.; Sirkis, J.S.; Baldwin, C.S.; Troll, J.R.; Grande, R.; Davis, C.S.; Vandiver, T.L. Embedded Fiber Optic Sensor Arrays for Structural Health Monitoring of Filament Wound Composite Pressure Vessels. In Proceedings of the Smart Structures and Materials 1999: Sensory Phenomena and Measurement Instrumentation for Smart Structures and Materials, Newport Beach, CA, USA, 31 May 1999. [[CrossRef](#)]
35. Kang, H.-K.; Park, J.-S.; Kang, D.-H.; Kim, C.-U.; Hong, C.-S.; Kim, C.-G. Strain monitoring of a filament wound composite tank using fiber Bragg grating sensors. *Smart Mater. Struct.* **2002**, *11*, 848–853. [[CrossRef](#)]
36. Kunzler, M.; Udd, E.; Kreger, S.; Johnson, M.; Henrie, V. Damage evaluation and analysis of composite pressure vessels using fiber Bragg gratings to determine structural health. In Proceedings of the Fiber Optic Sensor Technology and Applications IV, Boston, MA, USA, 23–26 October 2005. [[CrossRef](#)]
37. Yu, F.; Yin, S. (Eds.) *Fiber Optic Sensors*; CRC Press: Boca Raton, FL, USA, 2002; Volume 20020456, ISBN 978-0-8247-0732-3.
38. Haber, T.C.; Ferguson, S.; Guthrie, D.; Graver, T.W.; Soller, B.J.; Mendez, A. Analysis, compensation, and correction of temperature effects on FBG strain sensors. In Proceedings of the Fiber Optic Sensors and Applications X, Baltimore, MD, USA, 29 May 2013. [[CrossRef](#)]
39. Schreier, H.; Orteu, J.-J.; Sutton, M.A. *Image Correlation for Shape, Motion and Deformation Measurements*; Springer: Boston, MA, USA, 2009; ISBN 978-0-387-78746-6.
40. Pan, B. Recent Progress in Digital Image Correlation. *Exp. Mech.* **2011**, *51*, 1223–1235. [[CrossRef](#)]
41. Orteu, J.-J. 3-D computer vision in experimental mechanics. *Opt. Lasers Eng.* **2009**, *47*, 282–291. [[CrossRef](#)]
42. Clough, R.W. The finite element method in plane stress analysis. In Proceedings of the 2nd ASCE Conference on Electronic Computation, Pittsburgh, PA, USA, 8–9 September 1960.
43. Clough, R.W. Original formulation of the finite element method. *Finite Elem. Anal. Des.* **1990**, *7*, 89–101. [[CrossRef](#)]